1 **Analysis of the H-Ras mobility pattern *in vivo* shows cellular hetero-**

2 **geneity inside epidermal tissue**

3

4 Radoslaw J. Gora[1], Babette de Jong[2], Patrick van Hage[1], Mary A. Rhiemus[1], Fjodor van Steenis[1],

5 John van Noort[2], Thomas Schmidt[2], Marcel J.M. Schaaf[1*]

6

7

8 [1] Animal Sciences and Health Cluster, Institute of Biology, Leiden University, Leiden, The Netherlands.

9 [2] Biological, Soft and Complex Systems, Leiden Institute of Physics, Leiden University, Leiden, The Netherlands.

10 [*] Corresponding author. Animal Sciences and Health Cluster, Institute of Biology, Leiden University, Einsteinweg

11 55, 2333CC Leiden, The Netherlands. m.j.m.schaaf@biology.leidenuniv.nl.

12

13

14

15

16 **SUMMARY STATEMENT**

17 By application of single-molecule microscopy to living zebrafish embryos, factors altering the

18 *in vivo* dynamics of H-Ras proteins in epidermal cells were analyzed.

19

ABSTRACT

Over the last two decades, developments in single-molecule microscopy (SMM) have enabled imaging and tracking of individual, fluorescently labelled proteins in biological systems, and most of these studies have focused on the analysis of protein mobility patterns inside cultured cells. In the present study, SMM was applied *in vivo*, using the zebrafish embryo model. We studied the protein dynamics of the membrane protein H-Ras, mutants of this protein, and its membrane-anchoring domain, C10H-Ras, in epidermal cells of living two-day-old embryos, using a total internal reflection fluorescence microscopy (TIRFM) setup. For all proteins studied, our results consistently confirm the presence of a fast- and a slow-diffusing subpopulations of molecules, which both confine to microdomains within the plasma membrane. Although the mobility patterns of H-Ras, mutants of this proteins and its membrane-anchoring domain were remarkably similar, the constitutively active H-Ras mutant, H-Ras^{V12}, exhibited significantly higher diffusion rates than the wild-type H-Ras and its inactive mutant, H-Ras^{N17}. Ultimately, we characterized variability in our data obtained using the zebrafish embryo model and demonstrated that differences between cells within the same embryo are the largest source of variation in our data. Our findings are in line with a model in which the cellular architecture of individual cells within a tissue determine the mobility of H-Ras proteins anchored in the plasma membrane cytoplasmic leaflet. Thereby, our results underline the growing importance of performing SMM imaging *in vivo* in order to better understand factors influencing the protein dynamics in an intact living organism.

Keywords: H-Ras, zebrafish, single-molecule microscopy, total internal reflection fluorescence microscopy, membrane microdomains, diffusion

INTRODUCTION

45

46 Plasma membranes mostly consist of proteins and lipids that move laterally within the fluidic

47 membrane plane and interact with each other in both random and organized manners (Singer

48 and Nicolson, 1972). Until now, it has remained unclear what the origins are of many of such

49 interactions and how the organization and mobility of all membrane constituents are gov-

50 erned (Gheber, 2018). Furthermore, not much is known about the role of structural com-

51 plexes, such as the subjacent actomyosin cortex, in the dynamics of proteins and lipids in the

52 plasma membrane. Subsequently, definitions of membrane domains and their sizes remain

53 inconsistent. These domains include clathrin-coated pits and lipid rafts, and are believed to

54 compartmentalize the membrane, facilitate the assembly of signaling complexes, and serve

55 as the platforms for response amplification to the extracellular signaling molecules (Kusumi

56 et al., 2012). For instance, it is now estimated that lipid rafts, cholesterol-enriched membrane

57 domains, are predominantly transient complexes of 10-200 nm in size. Such lipid rafts are able

58 to adjust their size and stability in response to ongoing membrane trafficking or signal trans-

59 duction processes (Eggeling et al., 2009; Jacobson et al., 2019).

60

61 An important signaling protein that is present in the plasma membrane of many cell types in

62 vertebrate organisms is H-Ras. The H-Ras protein is a member of the Ras protein family, which

63 consists of small GTPases that activate intracellular signaling cascades, and thereby regulate

64 crucial biological processes taking place in various cells, such as growth, proliferation, and dif-

65 ferentiation (Malumbres and Barbacid, 2003). Gain-of-function mutations in genes encoding

66 Ras proteins are found in ca. 25% of human cancers, which makes Ras proteins interesting

67 targets of cancer therapies (Hobbs et al., 2016). These proteins are mainly localized at the

68 plasma membrane, though some fractions have also been reported to be present in mem-

69 branes of endosomes, the endoplasmic reticulum, and Golgi apparatus. Various Ras isoforms

70 exist, which differ predominantly in their so-called hyper variable region (HVR), formed by 25

71 amino acids present in their carboxyl-terminal end. The most carboxyl-terminal part of the

72 HVR comprises an anchoring domain, which is responsible for anchoring Ras proteins in the

73 cytoplasmic leaflet of the cell membranes upon posttranslational modifications, mostly the

74   addition of lipid groups. In H-Ras, this domain comprises a CAAX motif, which can be farnesyl-

75   ated, and two cysteine residues that can be (reversibly) palmitoylated (Brunsveld et al., 2009;

76   Willumsen et al., 1984).

77

78   Single-molecule microscopy (SMM) has been used in many studies to visualize individual mol-

79   ecules in the plasma membrane to study and characterize their organization and mobility. This

80   technique is mostly performed using advanced fluorescence microscope techniques, such as

81   light sheet fluorescence microscopy (LSFM) or total internal reflection fluorescence micros-

82   copy (TIRFM). The used microscopy setups are equipped with a laser for excitation of the flu-

83   orescent molecules and with a highly sensitive charged-couple device (CCD) or a complemen-

84   tary metal oxide semiconductor (CMOS) camera for capturing the emitted photons. Molecules

85   subjected to SMM experimentation are often fluorescently labeled. There are several options

86   for selecting a suitable fluorescent label, based on the biological model used or a spectrum of

87   excitation laser light available in the setup (Chudakov et al., 2010; Harms et al., 2001; Seefeldt

88   et al., 2008). Most often, autofluorescent proteins, such as Green or Yellow Fluorescent Pro-

89   teins (GFP, YFP) fused with an endogenous protein, are used, as they are not toxic to living

90   organisms and their use does not require permeabilization or fixation of the cells.

91

92   The mobility of Ras proteins or Ras membrane anchors fused to autofluorescent proteins has

93   been extensively studied and characterized by SMM in cultured cells (Lommerse et al., 2004;

94   Lommerse et al., 2005), with a positional accuracy of up to 30 nm and a temporal resolution

95   in the span from 5 to 50 milliseconds (Harms et al., 1999; Lommerse et al., 2004). Studies in

96   which the H-Ras anchoring domain and full-length H-Ras protein were fused with YFP (referred

97   to as YFP-C10H-Ras and YFP-H-Ras, respectively), showed that the anchor exhibits similar mo-

98   bility patterns to other anchors of human Ras proteins (e.g. K-Ras), and to the full-length H-

99   Ras protein (Lommerse et al., 2006). It was demonstrated that these protein populations seg-

100   regate into a slow- and a fast-diffusing fraction. The slow-diffusing fraction of the YFP-fused

101   anchors was found to confine to ca. 200 nm domains, whereas the full-length was only found

102   confined in such domains upon insulin-induced activation and mutation of the protein that

103   induces constitutive activation (YFP-H-Ras^{V12}) (Lommerse et al., 2004; Lommerse et al., 2005).

104

105   Studying cultured cells has the advantage of easier control and manipulation when compared
106   to living organisms. Nevertheless, studies using cultured cell models do not take into consid-
107   eration the influence of cell-cell interactions and extracellular stimuli that are present within
108   a tissue. Furthermore, they do not take into account factors an entire organism might be pre-
109   sented with that alter the context of the cells under investigation, such as changes due to the
110   diurnal cycle or the response to a stressor. Therefore, in order to perform SMM studies with
111   more translational value, we extended the applicability of the single-molecule research to a
112   more physiologically relevant system, using the zebrafish embryo as a model organism for
113   studying protein mobility patterns *in vivo*. Zebrafish embryos serve as excellent model organ-
114   isms for visual analyses of physiological processes, due to their optical clarity (Canedo and
115   Rocha, 2021; Detrich et al., 2011; Garcia et al., 2016; Gore et al., 2018; Lieschke and Currie,
116   2007). The high fecundity and short generation time of the zebrafish facilitate genetic screens
117   and identification of mutant phenotypes (Haffter et al., 1996; Reisser et al., 2018). Apart from
118   that, genetically modified zebrafish embryos can be readily created by use of microinjection
119   techniques, which makes this organism an excellent model for research using fluorescently
120   labeled cells and proteins.

121

122   In a previous study, we used a TIRFM-based approach to perform SMM in zebrafish, and we
123   analyzed the dynamics of YFP-C10H-Ras in epidermal cells of two-day-old embryos. The ob-
124   served mobility patterns in the zebrafish embryos were different from those found in cultured
125   cells, which underlined the importance of performing this type of studies *in vivo*. Therefore,
126   in the present study, we have extended this application of the *in vivo* SMM technique to the
127   full-length H-Ras protein. In addition to the wild type protein, we have used a constitutively
128   active and inactive H-Ras mutant (H-Ras^{V12} and H-Ras^{N17}, respectively) to examine how the
129   protein activity influences the patterns of diffusion and confinement of the H-Ras molecules.
130   Furthermore, we have studied the alterations in the mobility pattern during embryonic devel-
131   opment and performed experiments with YFP-C10H-Ras and the full-length H-Ras in human
132   embryonic kidney cells (HEK293T) to compare the results obtained in the zebrafish embryos
133   with results obtained in cultured cells using the same experimental protocol.

134

135   Our findings reveal that for YFP-C10H-Ras, YFP-H-Ras, YFP-H-Ras^{V12} and YFP-H-Ras^{N17}, in epi-

136   dermal cells of the zebrafish embryos and in cultured HEK293T cells, a slow- and a fast-diffus-

137   ing population of molecules can be distinguished and that both populations show confined

138   diffusion. Minor differences in the sizes of the populations, diffusion coefficients and confine-

139   ment sizes were detected between the proteins and models studied. Interestingly, in zebrafish

140   embryos, the mobility pattern does not change during embryonic development and the vari-

141   ability between individual embryos is smaller than the variability between different areas in

142   the epidermis of one embryo.

143

144   **RESULTS**

145   *The mobility pattern of YFP-C10H-Ras and YFP-H-Ras in HEK293T cells*

146

147   As an initial step in our SMM study, the YFP fusion proteins of the H-Ras anchoring domain

148   and full-length H-Ras protein (YFP-C10H-Ras and YFP-H-Ras respectively) were studied in cul-

149   tured HEK293T cells using our TIRFM setup. These experiments aimed to compare findings

150   obtained using the TIRFM setup with data previously obtained in cell cultures (Bobroff, 1986;

151   Lommerse et al., 2005), and with our previous findings in zebrafish embryos (Schaaf et al.,

152   2009). Prior to the SMM imaging, cells were transiently transfected with YFP-C10H-Ras and

153   YFP-H-Ras expression vectors and screened in order to analyze the expression levels and sub-

154   cellular localization of the fluorescent proteins. Images of HEK293T cells expressing YFP-C10H-

155   Ras, obtained through confocal laser scanning microscopy, indicated predominant membrane

156   localization of the signal coming from the YFP fused with the C10H-Ras membrane anchor,

157   which is in line with patterns observed before in mouse fibroblast and human embryonic kid-

158   ney cells (3T3-A14 and ts201, respectively) (Lommerse et al., 2004; Lommerse et al., 2005).

159

160   Three days after transfection, YFP-C10H-Ras and YFP-H-Ras expression levels in HEK293T cells

161   were significantly decreased. The sparse distribution allowed for identification of single YFP-

162   C10H-Ras molecules in the basal cell membrane, using our TIRFM setup. Diffraction-limited

163   fluorescence intensity peaks were observed and Gaussian curves were fitted over these peaks

164   (Fig. 1A, B). FWHM and intensity values of the Gaussian distributions corresponding to signals

165   from single YFP molecules were established in fixed HEK293T cells, taking into consideration

166   only these molecules that displayed single-step photobleaching, indicating that their signal

167   originated from an individual YFP molecule. These values were subsequently used to deter-

168   mine cutoff values for peak selection. The signal-to-noise ratio (SNR), defined as the quotient

169   between the average intensity of a single fluorophore (2215 counts) and the standard devia-

170   tion of the background signal (74 counts), approximated to 30. The positional accuracy

171   equaled approximately 22 nm in one dimension for the localization of these single molecules.

172

173   Image sequences were acquired using a time lag of 25 milliseconds, and the mobility pattern

174   of the proteins was determined by Particle Image Correlation Spectroscopy (PICS) software

175   (Semrau and Schmidt, 2007). Using a multistep analysis, information was yielded for five dif-

176   ferent time lags: 25, 50, 75, 100, and 125 milliseconds. By means of the PICS software, corre-

177   lations between the location of molecules in consecutive frames were determined, and cumu-

178   lative probability distributions of the displacements were generated for each time lag. The

179   data were then fitted to a one- or two-population model (Fig. 1C). The two-population model

180   fitted significantly better, indicating the presence of two fractions of molecules with different

181   mobility patterns. Using these curves, the relative size of the fast-diffusing fraction (α) and the

182   mean squared displacements of the fast and slow diffusing fractions (r_1^2 and r_2^2) were estab-

183   lished for each time lag.

184

185   Subsequently, for both YFP-C10H-Ras and YFP-H-Ras, the parameters α, r_1^2 , and r_2^2 were plot-

186   ted against the chosen time lags (Fig. 2). The relative size of the fast-diffusing fraction α was

187   constant over all time lags, and equaled 77.8 ± 0.4 % and 78.0 ± 0.5 % for YFP-C10H-Ras and

188   YFP-H-Ras, respectively. The curves presenting the relationship between mean squared dis-

189   placements (r_1^2 , and r_2^2) and the time lag for the fast and slow diffusing fractions are non-

190   linear and reach a plateau. We therefore fitted these curves using a confined diffusion model,

191   in which the movement of YFP-C10H-Ras and YFP-H-Ras is confined within an area of size L

192   with an initial diffusion coefficient D_0 (Bobroff, 1986; Lingwood and Simons, 2010; Schaaf et

193   al., 2009). The mobility patterns of the two fusion proteins were remarkably similar. For YFP-

194   C10H-Ras, D_0 of the fast-diffusing fraction equaled 1.40 ± 0.20 μm^2 s^{-1} and the size of the

195   confinement area L equaled 480 ± 7 nm. For YFP-H-Ras, the fast-diffusing fraction had a D_0

196   of 1.22 ± 0.13 μm^2 s^{-1} and was confined in an area of which L equaled 576 ± 11 nm. The

197   slow-diffusing fractions of YFP-C10H-Ras and YFP-H-Ras moved dramatically slower (D_0 of

198    $0.158 \pm 0.056 \ \mu m^2 \ s^{-1}$ and $0.173 \pm 0.036 \ \mu m^2 \ s^{-1}$) and were confined in smaller areas (L of

199   157 ± 5 nm and 219 ± 8 nm).

200

201   *The mobility pattern of YFP-C10H-Ras and YFP-H-Ras in epidermal cells of zebrafish embryos*

202

203   In order to successfully image membrane proteins in living zebrafish embryos, we focused our

204   observation on the outer epidermal cell layer in the tail fin of 2 dpf zebrafish embryos (Fig. 3).

205   Embryos were injected with DNA constructs of both YFP-C10H-Ras and YFP-H-Ras at the one-

206   cell stage in order to stably express the YFP-tagged H-Ras anchor and the full-length H-Ras

207   protein in the zebrafish tail fin. This outer cell layer of the skin (the superficial stratum) is a

208   homogenous layer of living cells, and forms the upper part of the skin (the epidermis) together

209   with an underlying cell layer. The homogeneity of this layer was illustrated by confocal micro-

210   scopic images of 2 dpf embryos of a transgenic zebrafish line expressing GFP-C10H-Ras in all

211   cells.

212

213   The tail fins of 2 dpf zebrafish embryos are morphologically stable enough to resist coverage

214   with a 0.75-mm-thick sheet of agarose, which was used in order to gently press the tail fin

215   towards the surface. This enables the evanescent field to excite the fluorophores present in

216   the outer membrane of cells in the outer epidermal cell layer. For imaging, we focused on the

217   tail fin region of the zebrafish embryo, while the rest of the zebrafish body was immersed in a

218   drop of water. Zebrafish vital functions, such as heartbeat and the blood flow in the cardio-

219   vascular system, were checked under a stereofluorescence microscope post-imaging.

220

221   As in HEK293T cells, we observed fast- and slow-diffusing protein fractions in zebrafish em-

222   bryos (Fig. 4). The fast-diffusing fraction size α equaled 65.0 ± 0.5 % for the YFP-C10H-Ras, and

223   65.9 ± 0.6 % for YFP-H-Ras. In both of the fractions, molecules followed a confined diffusion

224   pattern, with sizes of the confinement areas L for the fast-diffusing fractions being approxi-

225   mately 3-4 times larger than for the slow-diffusing ones (See Table 1, part 1.1, 1.2). The initial

226   diffusion coefficient D_0 of the fast-diffusing fraction equaled $1.10 \pm 0.15 \ \mu m^2 \ s^{-1}$ for YFP-

227   C10H-Ras and $0.71 \pm 0.05 \ \mu m^2 \ s^{-1}$ for YFP-H-Ras. The initial diffusion coefficients for the slow-

228 diffusing fractions were at least 8 times lower than the ones for their fast-diffusing counter-

229 parts. Overall, the results show that there is not a significant difference between HEK293T and

230 zebrafish embryo models, where we determine the mobility patters of YFP-H-Ras and YFP-

231 C10H-Ras, with a notable exception of the initial diffusion coefficients D_0 for YFP-H-Ras, which,

232 both in the case of the fast- and the slow-diffusing fraction, were significantly lower in the

233 zebrafish embryo model (See Table 1).

234

235 *The mobility pattern of YFP-C10H-Ras in zebrafish embryos at different developmental stages*

236

237 To study the stability of the data obtained in the zebrafish embryos over different develop-

238 mental stages, we analyzed the mobility patterns of YFP-C10H-Ras at 48, 56, 72 and 80 hpf. At

239 each stage, the values for the parameters α, r_1^2 , and r_2^2 were determined for each time lag,

240 and D_0 and L were determined for both fast- and slow-diffusing populations (Fig. 5). The re-

241 sults showed that a difference in the developmental stage of the zebrafish embryo did not

242 significantly influence any of these parameters (Table 2). This means that the C10H-Ras mo-

243 bility patterns remain stable within the time frame of our experiments.

244

245 *The mobility pattern of YFP-H-Ras^{V12} and YFP-H-Ras^{N17} in epidermal cells of zebrafish embryos*

246

247 To study the effect of the activation state of the H-Ras protein, the constitutively active H-

248 Ras^{V12} mutant (with a valine replacing a glycine at position 12) and the inactive mutant H-

249 Ras^{N17} (with an asparagine replacing a serine at position 17) were used. The fusion proteins

250 YFP-H-Ras, YFP-H-Ras^{V12} and YFP-H-Ras^{N17} were expressed in 2 dpf zebrafish embryos, and the

251 mobility patterns of the each of these constructs were analyzed. Again, we observed a fast-

252 and a slow-diffusing fractions of molecules. The size of the fast-diffusing fraction did not differ

253 significantly between the constructs, and equaled 66.0 ± 0.5 % for YFP-H-Ras, 61.7 ± 0.7 % for

254 YFP-H-Ras^{V12}, and 63.2 ± 0.2 % for YFP-H-Ras^{N17} (Fig. 6A). All fractions showed confined diffu-

255 sion. Initial diffusion coefficients D_0 for the fast-diffusing fraction equaled 0.70 ± 0.05

256 $\mu m^2\ s^{-1}$ for YFP-H-Ras, 1.05 ± 0.06 $\mu m^2\ s^{-1}$ for YFP-H-Ras^{V12}, and $0.72 \pm 0.07\ \mu m^2\ s^{-1}$ for

257 YFP-H-Ras^{N17}, with the diffusion coefficient for YFP-H-Ras^{V12} being significantly higher than

258 that for the other two constructs (Fig. 6B). Similarly, the size of the confinement area L for

259 YFP-H-Ras^{V12} (572 ± 7 nm) was significantly higher than those for YFP-H-Ras and YFP-H-Ras^{N17}

260 (421 ± 8 nm and 444 ± 9 nm, respectively). The initial diffusion coefficients and the sizes of

261 the confinement areas for the slow diffusing fractions of YFP-H-Ras^{V12} and YFP-H-Ras^{N17} did

262 not show any significant difference from the values determined for the wild type YFP-H-Ras

263 (0.022 ± 0.003 μm^2 s^{-1} and 103 ± 5 nm; for detailed results, see Table 1, Table 2, and Fig. 6C).

264

265 **TABLE 1.** *Results of the analysis of the mobility patterns of YFP-C10H-Ras, YFP-H-Ras, YFP-H-Ras^{V12}, YFP-H-Ras^{N1}*

Experiment	D_{0FD} [$\mu m^2\ s^{-1}$]	D_{0SD} [$\mu m^2\ s^{-1}$]	L_{FD} [nm]	L_{SD} [nm]	α [%]
YFP-C10H-Ras: comparison between HEK293T cells and zebrafish embryos					
HEK293T	1.40 ± 0.20	0.158 ± 0.056	480 ± 7	157 ± 5	77.8 ± 0.4
zebrafish	1.10 ± 0.15	0.128 ± 0.057	467 ± 9	147 ± 6	65.0 ± 0.5
YFP-H-Ras: comparison between HEK293T cells and zebrafish embryos					
HEK293T	1.22 ± 0.13	0.173 ± 0.036	576 ± 11	219 ± 8	78.0 ± 0.5
zebrafish*	0.71 ± 0.05	0.022 ± 0.003	421 ± 8	103 ± 5	65.9 ± 0.6
YFP-C10H-Ras in zebrafish embryos: developmental study					
48 hpf	1.84 ± 0.44	0.114 ± 0.036	507 ± 10	170 ± 7	68.2 ± 1.3
56 hpf	1.54 ± 0.07	0.199 ± 0.047	610 ± 5	197 ± 6	60.6 ± 0.5
72 hpf	1.27 ± 0.04	0.128 ± 0.032	616 ± 3	124 ± 2	62.9 ± 0.4
80 hpf	1.10 ± 0.20	0.107 ± 0.026	572 ± 19	153 ± 3	52.4 ± 0.4
YFP-H-Ras$^{(WT, N17, V12)}$ in zebrafish embryos: comparison of the mutants					
YFP-H-Ras	0.71 ± 0.05	0.022 ± 0.003	421 ± 8	103 ± 5	65.9 ± 0.6
YFP-H-Ras^{N17}	0.72 ± 0.07	0.030 ± 0.002	444 ± 9	100 ± 2	63.2 ± 0.1
YFP-H-Ras^{V12}	1.05 ± 0.06	0.055 ± 0.006	572 ± 7	132 ± 5	61.8 ± 0.8

266 *Results of YFP-H-Ras used for comparison between the models are taken from experiment in which YFP-H-Ras, YFP-H-Ras^{V12}*

267 *and YFP-H-Ras^{N17} were studied.*

268

269 *The sources of variability of the results*

270

271 Finally, we analyzed the sources of variability of the results obtained in zebrafish embryos for

272 YFP-H-Ras and the two mutants, YFP-H-Ras^{V12} and YFP-H-Ras^{N17}. For this purpose, we first

273 studied the correlation between the number of individual molecules within images and the

274 parameters α, r_1^2, and r_2^2. Correlation coefficients between the number of molecules and the

275 corresponding parameters were low (0.22, 0.19 and 0.28, respectively), indicating that the

276 correlation between the number of molecules in an image and the parameters describing pro-

277 tein mobility is very weak. Thus, we affirm that the number of molecules has a negligible im-

278 pact on the H-Ras mobility analysis.

279

280 **TABLE 2.** *Statistical analysis performed for the values of mean squared displacements and fast-diffusing fraction sizes obtained*

281 *experimentally for the 25 ms time lag.*

Statistical significance	Mean squared displacement: Fast-diffusing fraction (r_1^2)	Mean squared displacement: Slow-diffusing fraction (r_2^2)	Fraction size: fast-diffusing fraction (α)
YFP-C10H-Ras: HEK293T cells vs zebrafish embryo[1]	P > 0.05, NS	P > 0.05, NS	P > 0.05, NS
YFP-H-Ras: HEK293T cells vs zebrafish embryo[1]	P < 0,001, ****	P < 0,001, ****	P > 0.05, NS
YFP-C10H-Ras in zebrafish embryos: developmental stage[2]	P > 0.05, NS	P > 0.05, NS	P > 0.05, NS
YFP-H-Ras, YFP-H-Ras[V12] and YFP-H-Ras[17] in zebrafish embryos[2]	P(WT, N17) > 0.05, NS P(WT, V12) < 0,001, **** P(N17, V12) < 0.001, ****	P(WT, N17) > 0.05, NS P(WT, V12) = 0.016, * P(N17, V12) = 0.011, *	P > 0.05, NS

282 [1]*For comparisons between two biological models, HEK293T cells and zebrafish embryos, an unpaired t-test was used.*

283 [2]*For comparisons of protein mobility patterns in zebrafish embryos at different developmental stages as well as for compari-*

284 *sons between genetic mutants of YFP-H-Ras, a one-way ANOVA was used. In case the differences between groups were sig-*

285 *nificant in the one-way ANOVA, results of multiple groups comparison are shown, performed by a Tukey post-hoc test.*

286 *NS, non-significant (P>0.05); *, P<0.05; ****, P<0.001.*

287

288 **TABLE 3.** *Summary of the variance values (σ^2) per source parameter and their percentage contribution (%) towards the total*

289 *variance for the given parameter.*

Source of variation	α		r_1^2		r_2^2	
	σ^2	%	σ^2	%	σ^2	%
Experimental Day	0.188	33.1	0.097	49.2	0.111	35.6
Embryo	0.122	21.5	0.018	9.0	0.004	1.4
Imaging Area	0.173	30.4	0.066	33.7	0.157	50.5
Residual[1]	0.085	14.9	0.016	8.1	0.039	12.5

290 [1]*Residuals account for variance that cannot be explained by the experimental design.*

291

292 Secondly, the contribution of three factors to the overall variability in the results was analyzed.

293 These factors were: the different batches of zebrafish embryos, different individual embryos,

294 and the different imaged areas. By use of hierarchical linear mixed models, we generated cat-

295 erpillar plots for α, r_1^2 , and r_2^2 , which present random effects distribution, being the deviation

296 of the group intercept from an overall mean, and the contribution of each of the three factors

297 to the overall mean of a given parameter (Fig. 6D-F). Subsequently, we quantified the percent-

298 age contribution of each of the selected sources of variation towards the overall data variabil-

299 ity (Table 3). These caterpillar plots and the quantitative source of variation analysis both show

300 that, for every parameter, most of the random effects come from imaging embryos on differ-

301 ent experimental days (contribution to the total variability of 33.1% for the fraction size, 49.2%

302 for the fast-diffusing fraction diffusion coefficient) and imaging different areas within the ep-

303 idermis of the same zebrafish embryo (contribution of 50.1% for the slow-diffusing subpopu-

304 lation diffusion coefficient). Interestingly, imaging different embryos from the same batch was

305 the smallest source of variability for all parameters, and did not introduce nearly as much

306 variability as imaging of different areas within the same individual zebrafish embryo (Table 3).

307

308 **DISCUSSION**

309 In the present study, we have applied single-molecule microscopy to an *in vivo* model system,

310 using living zebrafish embryos. As our model molecule we have used a YFP-fusion of H-Ras, a

311 signaling protein that is anchored in the cytoplasmic leaflet of the plasma membrane. Based

312 on the observed mobility patterns in epidermal cells of the embryos, two fractions of H-Ras

313 molecules were distinguished: a fast- and a slow-diffusing one, which both show confined dif-

314 fusion. The fast fraction contains the majority of molecules and shows an initial diffusion co-

315 efficient that is approximately 10 to 15 times higher than that of the slow-diffusing fraction.

316 Similar mobility patterns were obtained when only the membrane anchor of the H-Ras protein

317 was fused to YFP, or when a constitutively inactive H-Ras mutant (H-Ras^{N17}) was studied. A

318 constitutively active H-Ras mutant (H-Ras^{V17}), however, showed an increased mobility with a

319 higher diffusion coefficient and a larger confinement area. Interestingly, the largest variation

320 in these experiments was not found between individual embryos, but between different ex-

321 perimental days and the areas within a single embryo.

322

323 In this study, the observation of a fast and a slow diffusing fraction of H-Ras molecules that

324 were both confined was highly consistent between experimental models used, i.e., between

325 cultured human embryonic kidney (HEK293T) cells and epidermal cells of zebrafish embryos,

326 between different stages of zebrafish embryonic development, and between the full length

327   H-Ras protein, the constitutively active and inactive mutant and the H-Ras membrane anchor

328   (C10H-Ras). These fast and slow diffusing fractions have been found before in several single-

329   molecule microscopy studies on H-Ras or C10H-Ras (the latter also in zebrafish embryos), with

330   diffusion coefficients comparable to those found in the present study (Lommerse et al., 2004;

331   Lommerse et al., 2005; Lommerse et al., 2006; Schaaf et al., 2009). However, confinement of

332   these fractions was not always observed, which in most cases may have been due to the

333   shorter time ranges used in these studies combined with larger variation or smaller sample

334   sizes.

335

336   Although the observed mobility patterns were remarkably stable in our experiments, we did

337   observe two cases of altered mobility. First, the full-length H-Ras protein displayed a lower

338   diffusion coefficient in the epidermal cells of the embryos compared to the diffusion coeffi-

339   cients found in the HEK293T cells. This difference was observed for both fractions of this pro-

340   tein, but was not found for any of the fractions of the C10H-Ras protein. Second, the consti-

341   tutively active H-Ras mutant protein H-Ras[V17] showed increased mobility of its fast-diffusing

342   fraction compared to the wild type H-Ras protein, which was reflected in an increased initial

343   diffusion coefficient and a larger confinement area compared to the wild type H-Ras protein.

344   In a previous study on the mobility of this mutant in cultured mouse embryonic fibroblasts

345   (3T3 cells), this increased mobility was not observed (Lommerse et al., 2006). In addition to

346   the shorter time range, larger variation and smaller sample sizes mentioned earlier as an ex-

347   planation for such discrepancies, the cell type used may be also be a possible factor underlying

348   the absence of this effect in the earlier study.

349

350   Using the mobility data obtained in zebrafish embryos, we studied the factors that contributed

351   to the variation in these data. Interestingly, differences between individual embryos only had

352   a modest effect on the overall variation in the results. However, different experimental days

353   and different areas of the embryonic epidermis that we imaged both appeared to be factors

354   that showed large contribution to the overall variation in the data. The area that we imaged

355   had a size of 16.6x16.6 μm, which is approximately the area of a single cell (see Fig. 3), so we

356   assume that cell-to-cell variation within the epidermal tissue was a main source of the ob-

357   served variation. This indicates that the cellular context determines H-Ras mobility, and that

358   differences between cells within the epidermal tissue of one individual embryo are larger than

13

359 the differences in average cellular context in the tissue between embryos. The observation

360 that the membrane anchor of H-Ras fused to YFP (C10H-Ras) shows a mobility pattern similar

361 to the full length YFP-H-Ras fusion protein indicates that the functionality of the protein does

362 not play a role and that therefore interactions with structural elements of the cell, such as

363 specific membrane domains and the cytoskeleton, are determining the dynamics of these pro-

364 teins. In addition to the cell-to-cell variation, day-to-day variation appeared to contribute

365 largely to the total variation. We assert that these differences may for a large part originate

366 from an inherent variability between different zebrafish batches. The AB/TL zebrafish wild

367 type strain that was used is not an inbred strain, and its genetic heterogeneity might underlie

368 batch to batch variation. Furthermore, small differences in treatment conditions might affect

369 embryonic development, alter complex metabolic pathways, and induce stress responses, and

370 thereby cause, to some extent, the observed differences in the values of the measured dy-

371 namic parameters on different experimental days.

372

373 Lipid-tethered Ras protein family members have been reported to possess an intrinsic ability

374 to form nanoclusters composed by a small number of Ras molecules. It has been specifically

375 shown that H-Ras is localized in largely separated nanoclusters of less than 30 nm that have

376 an average lifetime of less than 1 second (Pezzarossa et al., 2015; Plowman et al., 2005; Prior

377 et al., 2003; Rotblat et al., 2004). It has been suggested that these clusters of H-Ras proteins

378 are localized in lipid rafts, which are thought to be cholesterol-enriched domains in the plasma

379 membrane from 10 to 100 nm in size (Garcia-Parajo et al., 2014; Lingwood and Simons, 2010;

380 Nickels et al., 2015). Due to the selective partitioning of rafts and the surrounding areas, rafts

381 are responsible for controlling specific downstream signaling processes, by enhancing certain

382 protein-protein interactions, while suppressing others. These relatively immobile H-Ras

383 nanoclusters are a result of temporal trapping within these domains and constitute approxi-

384 mately 40% of the total protein population, whereas the rest of the H-Ras molecules remains

385 monomeric and laterally mobile within the plasma membrane (Dadke and Chernoff, 2003;

386 Murakoshi et al., 2004; Rotblat et al., 2004). In the current study, the fraction size of the fast-

387 diffusing H-Ras in living zebrafish embryos equaled approximately 35%, suggesting that this

388 fraction reflects the clustering subpopulation of H-Ras molecules. Thus, H-Ras compartmen-

389 talization into confinement areas within the plasma membrane is believed to be necessary to

390 aggregate a high number of H-Ras molecules in order to confine a cytoplasmic signal to an

391 area in which an extracellular signal is received (Simons and Gerl, 2010).

392

393 The localization of H-Ras in lipid rafts appears to be enhanced by the presence of the lipid

394 anchor (Pezzarossa et al., 2015; Rotblat et al., 2004) and in our study lipid anchor of H-Ras

395 indeed appears to be sufficient for the formation of the slow-diffusing fraction. In contrast, it

396 has been shown that GTP loading of the N-terminus of the protein decreases the affinity of H-

397 Ras for these microdomains (Rotblat et al., 2004). Relatively high diffusion coefficients have

398 been observed for the H-Ras^{V12} fast-diffusing fractions, which is in line with our results for this

399 mutant. The confinement of the fast-diffusing subpopulation may result from exclusion from

400 lipid rafts, but other cellular structures, such as the actin cytoskeleton, may play an equally

401 important role in confinement of membrane molecules. Multiple studies have suggested that

402 confinement areas can also be formed by impermeable barriers constituted by cytoskeleton

403 reformation. The membrane-associated cytoskeleton is a highly organized structure that is

404 able to create multimolecular membrane-cytoskeleton assemblies, including focal adhesions

405 and podosomes (Garcia-Parajo et al., 2014).

406

407 In conclusion, in the present study we have used a previously developed TIRFM-based ap-

408 proach to perform SMM in an intact vertebrate organism. Our study confirms that this tech-

409 nology is highly useful for studying the molecular behavior of individual receptors and signal-

410 ing molecules, and enables further *in vivo* studies to unravel exact molecular mechanisms gov-

411 erning molecular interactions and their role in physiological and pathological processes, such

412 as skin cancer, wound healing, or tissue regeneration (Kaufman et al., 2016; Kawakami et al.,

413 2004). We have studied the mobility pattern of H-Ras in the epidermis of living zebrafish em-

414 bryos, and our data show the consistent presence of a fast and a slow diffusing fraction of H-

415 Ras molecules, which both show confinement. Interestingly, the epidermal tissue shows a

416 large degree of heterogeneity between individual cells, and variation in the structural context

417 of cells within this tissue appears to be a main determinant of H-Ras dynamics.

418

419

MATERIAL AND METHODS

Zebrafish. Wild type ABTL zebrafish (*Danio rerio*) were grown and maintained according to standard protocols (http://ZFIN.org), exposed to a 14h light and 10h dark diurnal cycle at 28°C. Fertilization was performed by natural spawning at the beginning of the light period. Eggs were collected and raised in egg water (60 μg/ml Instant Ocean sea salts, Cincinnati, OH, USA) at 28°C. All experiments performed on living zebrafish embryos were done in compliance with the directives of the local animal welfare committee of Leiden University.

Cell cultures, transfection, and fixation. In all cell culture experiments, human embryonic kidney cells (HEK293T) were used. Cells were cultured in DMEM (Dulbecco's Modified Eagle Medium, Invitrogen, Waltham, MA, USA) supplemented with penicillin and streptomycin (10 μg ml^{-1}, Invitrogen), Glutamax (10 μg ml^{-1}, Invitrogen) and 10% fetal calf serum (Invitrogen) at 37°C in a humidified atmosphere containing 5% of CO_2. Cells were passaged every 3 to 4 days and kept in use for a maximum of 12 passages. Before transfection, cells were transferred onto a sterile, glass coverslip (diameter 25 mm, Marienfeld, Lauda-Königshofen, Germany) placed in a well of a 6-well plate. At a confluency level of 20-30%, cells were transfected with 1 μg of DNA per well, using FuGENE 6, according to the manufacturer's protocol (Roche Molecular Biochemicals, Indianapolis, USA). The transfection efficiency, determined by fluorescence microscopy screening at 48h after transfection (EVOS M7000 Cell Imaging Systems, ThermoScientific, Waltham, MA, USA), was approximately 30%. Cells were imaged at least 4 days post-transfection to lower the expression level of the YFP-fused proteins and to be able to efficiently observe single molecules. Prior to the single-molecule microscopy experiments, DMEM was replaced by PBS (phosphate-buffered saline; 150 mM NaCl, 10 mM Na_2HPO_4/NaH_2PO_4, pH 7.4) kept at room temperature. Finally, the coverslips with cells were mounted on a microscope holder, and 500 μl of room-temperature PBS was pipetted onto the cells. For single-step photobleaching experiments, transfected cells were fixed using 4% paraformaldehyde (PFA) in PBS overnight, at 4°C. Immediately before the experiments, the cells were washed three times, 5 minutes each time, with PBS. Finally, the cells were rinsed twice with PBST (PBS with Tween^{TM}-20, 0.1%), for 5 minutes each time.

16

450   *Microinjection of DNA in zebrafish embryos.* The cDNAs encoding YFP-C10H-Ras, YFP-H-Ras,

451   YFP-H-Ras^{V12}, and YFP-H-Ras^{N17} were cloned from pcDNA3.1(+) mammalian expression plas-

452   mids into pCS2(+) plasmids, which then served as vectors for expression of the fluorescent

453   proteins of interest. DNA plasmid microinjections were performed at concentration dose of

454   30 pg per embryo at the 1-2 cell stage, resulting in a mosaic expression of the fluorescent

455   protein in the zebrafish embryos at later stages. Microinjections were done using a Femtojet

456   microinjector (Eppendorf, Hamburg, Germany) and a micromanipulator with pulled microca-

457   pillary pipettes. The procedure of microinjections was controlled under a stereomicroscope

458   (M165C, Leica Microsystems, Wetzlar, Germany). Injected eggs were then left to develop in

459   an incubator at 28°C. Viability and development of the eggs after microinjections was checked

460   on a daily basis using fluorescence stereo- or confocal microscopy.

461

462   *Fluorescence stereomicroscopy.* For screening zebrafish embryos expressing YFP-fused pro-

463   teins, a Leica M205FA fluorescence stereomicroscope (Leica Microsystems) was used. Images

464   of the zebrafish embryos were taken using a Leica DFC 345FX camera.

465

466   *Confocal laser-scanning microsc*opy. A Leica SPE confocal laser-scanning microscope (Leica

467   Microsystems) was used to investigate the fluorescent signal in the zebrafish embryo. Excita-

468   tion was done using an argon laser at 514 nm. Images were obtained using a 20x and 40x non-

469   immersion objectives (NA 0.70, NA 0.80, respectively), and a 63x water immersion objective

470   (NA 1.20).

471

472   *Total internal reflection fluorescence microscopy (TIRFM).* Glass coverslips were washed with

473   99% ethanol (twice), HPLC-grade water (twice), KOH (1M, twice), and acetone (99%, thrice).

474   Each wash was followed by a 30-minute-long sonication period at 50°C. If not used immedi-

475   ately, the coverslips were stored in acetone. Prior to the mounting of the zebrafish embryos,

476   the glass coverslips were coated with 50 µg ml^{-1} of poly-L-lysine (Sigma-Aldrich, St. Louis, MO,

477   USA) for 5 minutes, followed by a double wash with deionized water and drying with nitrogen

478   gas. Two-day-old zebrafish embryos were equilibrated at room temperature for an hour,

479   anaesthetized with 0.02% aminobenzoic acid ethyl ester (tricaine, Sigma-Aldrich) and decho-

480   rionated using tweezers. Subsequently, a single zebrafish embryo was placed on a coverslip

17

481   with a lateral side against the coverslip, while excess water was aspirated. The tail of the em-

482   bryo was pressed against the surface of the coverslip by a thin agarose sheet (2%, thickness

483   0.75 mm). A drop of egg water was added to cover the rest of the embryo's body. The coverslip

484   with the embryo was placed on a microscope holder and mounted on the TIRFM setup. This

485   setup was a custom-made microscope with a 100x oil-immersion objective (NA 1.45, Nikon,

486   Tokyo, Japan). Excitation was performed using a 515 nm laser (iChrome MLE, Toptica Photon-

487   ics, Germany), the field of view was set to a 100x100 pixels region with a pixel size of 166 nm,

488   and the laser power equaled to 20% of the maximal laser power (40 mW). The incident laser

489   beam was set at the critical angle against the coverslip-water interface, thus being totally re-

490   flected and creating the evanescent wave for excitation of fluorophores close to the coverslip-

491   sample interface. Emission light was filtered using a long pass filter (ET5701p, Chroma Tech-

492   nology, VT, USA), and image sequences were collected using an on-chip multiplication gain

493   CCD camera (model 512B, Cascade, Roper Scientific, Tucson, AZ, USA). Each image sequence

494   contained 1200 frames separated by a 25 ms time lag, resulting in the total acquisition time

495   of 30 seconds.

496

497   *Analysis of protein diffusion patterns.* The analysis of the position of individual molecules was

498   done as described previously. Fluorescence intensity signals corresponding to YFP molecules

499   were fitted to a two-dimensional Gaussian surface, using previously custom-developed soft-

500   ware (Groeneweg et al., 2014; Lommerse et al., 2004; Lommerse et al., 2005). Subsequently,

501   the corresponding signals were filtered based on their full width at half maximum (FWHM)

502   value and their intensity count, based on the microscopy setup. The FWHM and intensity

503   threshold values were obtained in the single-step photobleaching experiments (performed

504   using fixed HEK293T cells), by averaging the Gaussian distributions of 20 different YFP mole-

505   cules in the last step prior to the photobleaching-induced final intensity drop (using TrackMate

506   plug-in, ImageJ). The location of a molecule was defined by the center of the Gaussian curve.

507   Positional accuracy (dx) of the peak localization equaled approximately 22 nm (Groeneweg et

508   al., 2014; Schütz et al., 1997).

509

510   To study the mobility pattern of the proteins, Particle Image Correlation Spectroscopy (PICS)

511   software was used, which has been previously described (Semrau and Schmidt, 2007). A mul-

512   tistep analysis was performed for each image sequence acquired, yielding information for five

513   different time lags of 25, 50, 75, 100, and 125 milliseconds. In PICS analysis, individual particles

514   are not tracked, but correlations between the location of molecules in consecutive frames are

515   determined. This way, cumulative probability distributions of the squared displacements were

516   generated for each of the time lags, and fitted to one- or two-population model. The former

517   is described by the equation:

518

519
$$P\left(r^2, t_{lag}\right) = 1 - exp\left(-\frac{r^2}{r_0^2\left(t_{lag}\right)}\right) \ (1)$$

520

521   which describes the probability that a particle exhibiting Brownian motion at the arbitrary

522   origin is found within a circle of a radius r at the time lag t_{lag}, and its mean square displace-

523   ment equals $r_0^2\left(t_{lag}\right) = 4Dt_{lag}$. However, in case that the populations of the molecules can

524   be differentiated into two different populations equation (1) is transformed into:

525

526
$$P\left(r^2, t_{lag}\right) = 1 - \left[\alpha \cdot exp\left(-\frac{r^2}{r_1^2\left(t_{lag}\right)}\right) + (1 - \alpha) \cdot exp\left(-\frac{r^2}{r_2^2\left(t_{lag}\right)}\right)\right] \ (2),$$

527

528   where the mean square displacement of fast-diffusing and slow-diffusing populations are de-

529   noted by r_1^2 and r_2^2, and their relative sizes by α and $1 - \alpha$, respectively (Schaaf et al., 2009).

530   Hence, α represents the fraction size of the fast-diffusing H-Ras molecules and is represented

531   as a percentage of the total population.

532

533   To examine whether any of these populations confine to a certain area, the values of r_1^2 and

534   r_2^2 were plotted against the time lag. For the larger time lags the variance increases due to the

535   smaller number of statistically independent measurements of r^2 (Kusumi et al., 1993). The

536   positional accuracy (dx) led to a constant offset in r^2 of $4 \cdot (dx)^2$, which, in our case, equaled

537   0.0049 μm². The plots were fitted by a free Brownian diffusion model, with a diffusion coeffi-

538   cient D in the fitted equation $r_i^2\left(t_{lag}\right) = 4Dt_{lag}$, or by a confined diffusion model described

539   by the equation:

540

541
$$r_i^2\left(t_{lag}\right) = \frac{L^2}{3} \cdot \left[1 - exp\left(-\frac{12 \cdot D_0 \cdot t_{lag}}{L^2}\right)\right] \ (3),$$

19

542

543 in which the molecules move freely with an initial diffusion coefficient D_0, but are confined by

544 impermeable barriers within an area described by a square of a side length L.

545

546 *Experimental design.* In every experiment, three different zebrafish embryos were selected

547 for the TIRF microscopy imaging. In each of the selected embryos, at least three separate areas

548 were imaged. The data shown reflect a minimum of three independent experiments, each

549 performed on three different days. Six independent experiments were done for YFP-C10H-Ras

550 (18 individual embryos), and three for the wild-type YFP-H-Ras, YFP-H-Ras[N17], and YFP-H-

551 Ras[V12] (9 individual embryos per H-Ras construct). For studying the influence of the develop-

552 mental stage on the YFP-C10H-Ras dynamics, an analogous design was implemented (3 exper-

553 iments, 3 individual embryos per each experiment), yet the embryos were selected and im-

554 aged at 48-, 56-, 72-, and 80-hour post fertilization. In the case of transfected HEK293T cells,

555 three independent experiments were performed for both YFP-C10H-Ras and wild-type YFP-H-

556 Ras. In each of those experiments, three different coverslips with growing cells were selected

557 from a 6-well-plate, and at least three different cells were imaged on each of the coverslips.

558

559 *Statistical Analysis.* Values of the fast-diffusing population sizes and squared displacements

560 were averaged per experimental day for each time lag in all individual groups (i.e., YFP-C10H-

561 Ras, YFP-H-Ras, YFP-H-Ras[N17], and YFP-H-Ras[V12]). Statistical analysis of the data (presented in

562 Table 2 for the 25 ms time lag) was performed for each time lag by comparing: (a) results

563 obtained from zebrafish embryos expressing wild-type YFP-H-Ras, YFP-H-Ras[N17], and YFP-H-

564 Ras[V12]; (b) results obtained for HEK293T cells expressing YFP-C10H-Ras and wild-type YFP-H-

565 Ras, (c) results obtained zebrafish embryos expressing YFP-C10H-Ras at 48-, 56-, 72-, and 80-

566 hour post fertilization. In addition, a comparison between biological models was performed,

567 using results obtained for YFP-C10H-Ras and wild-type YFP-H-Ras for both zebrafish embryos

568 and HEK293T cells. Intragroup variability analysis was carried out between all experimental

569 groups belonging to the same biological model and construct expressed. Initial diffusion coef-

570 ficients and confinement area sizes were obtained through a confined model fit, by pooling

571 and averaging values of mean square displacements for each individual H-Ras construct, bio-

572 logical model, and time post-fertilization.

573

574   In order to check if data were normally distributed, a Shapiro-Wilk statistical test was per-

575   formed. Significance of the results was performed using a Student's t-test for comparison of

576   means between two, normally distributed, groups. When multiple groups were compared, a

577   one-way ANOVA was implemented with a Tukey range test for post hoc analysis. Ultimately,

578   the source of potential variability of the data was examined by using a hierarchical linear

579   model to account for nested structure of the data (i.e., different areas within an embryo, dif-

580   ferent embryos within an experimental day). The values of the r^2 were logarithm-transformed

581   and the α logit-transformed to meet the hypotheses of the statistical model.

582

COMPETING INTERESTS

584   The authors declare no competing financial interests.

585

FUNDING

589

AUTHOR CONTRIBUTIONS

591   Conceptualization: M.J.M.S.; Methodology: R.J.G., B.J., M.A.R., T.S., M.J.M.S.; Software: R.J.G.,

592   B.J., P.H, J.N.; Validation: R.J.G., M.J.M.S.; Formal analysis: R.J.G., F.S., P.H.; Investigation:

593   R.J.G., M.A.R, F.S., P.H.; Resources: M.J.M.S.; Data curation: R.J.G., M.J.M.S.; Writing - original

594   draft: R.J.G., M.J.M.S.; Writing - review & editing: R.J.G., J.N., T.S., M.J.M.S.; Supervision:

595   M.J.M.S.; Project administration: M.J.M.S.; Funding acquisition: M.J.M.S.

596

597

598 **REFERENCES**

599 **Bobroff, N.** (1986). Position measurement with a resolution and noise-limited instrument.

600 *Rev. Sci. Instrum.* **57**, 1152–1157.

601 **Brunsveld, L., Waldmann, H. and Huster, D.** (2009). Membrane binding of lipidated Ras pep-

602 tides and proteins — The structural point of view. *Biochim. Biophys. Acta BBA -*

603 *Biomembr.* **1788**, 273–288.

604 **Canedo, A. and Rocha, T. L.** (2021). Zebrafish (Danio rerio) using as model for genotoxicity

605 and DNA repair assessments: Historical review, current status and trends. *Sci. Total*

606 *Environ.* **762**, 144084.

607 **Chudakov, D. M., Matz, M. V., Lukyanov, S. and Lukyanov, K. A.** (2010). Fluorescent Pro-

608 teins and Their Applications in Imaging Living Cells and Tissues. *Physiol. Rev.* **90**,

609 1103–1163.

610 **Dadke, S. and Chernoff, J.** (2003). Protein-tyrosine Phosphatase 1B Mediates the Effects of

611 Insulin on the Actin Cytoskeleton in Immortalized Fibroblasts*. *J. Biol. Chem.* **278**,

612 40607–40611.

613 **Detrich, H. W., III, H. W. D., Westerfield, M. and Zon, L. I.** (2011). *The Zebrafish: Genetics,*

614 *Genomics and Informatics*. Academic Press.

615 **Eggeling, C., Ringemann, C., Medda, R., Schwarzmann, G., Sandhoff, K., Polyakova, S., Be-**

616 **lov, V. N., Hein, B., von Middendorff, C., Schönle, A., et al.** (2009). Direct observa-

617 tion of the nanoscale dynamics of membrane lipids in a living cell. *Nature* **457**, 1159–

618 1162.

619 **Garcia, G. R., Noyes, P. D. and Tanguay, R. L.** (2016). Advancements in zebrafish applications

620 for 21st century toxicology. *Pharmacol. Ther.* **161**, 11–21.

621 **Garcia-Parajo, M. F., Cambi, A., Torreno-Pina, J. A., Thompson, N. and Jacobson, K.** (2014).

622 Nanoclustering as a dominant feature of plasma membrane organization. *J. Cell Sci.*

623 **127**, 4995–5005.

624 **Gheber, L. A.** (2018). The Life of a Membrane Protein. *Biophys. J.* **114**, 2762–2763.

625 **Gore, A. V., Pillay, L. M., Galanternik, M. V. and Weinstein, B. M.** (2018). The zebrafish: A
626   fintastic model for hematopoietic development and disease. *WIREs Dev. Biol.* **7**,
627   e312.

628 **Groeneweg, F. L., Royen, M. E. van, Fenz, S., Keizer, V. I. P., Geverts, B., Prins, J., Kloet, E. R.**
629   **de, Houtsmuller, A. B., Schmidt, T. S. and Schaaf, M. J. M.** (2014). Quantitation of
630   Glucocorticoid Receptor DNA-Binding Dynamics by Single-Molecule Microscopy and
631   FRAP. *PLOS ONE* **9**, e90532.

632 **Haffter, P., Granato, M., Brand, M., Mullins, M. C., Hammerschmidt, M., Kane, D. A., Oden-**
633   **thal, J., van Eeden, F. J., Jiang, Y. J., Heisenberg, C. P., et al.** (1996). The identification
634   of genes with unique and essential functions in the development of the zebrafish,
635   Danio rerio. *Development* **123**, 1–36.

636 **Harms, G. S., Sonnleitner, M., Schütz, G. J., Gruber, H. J. and Schmidt, Th.** (1999). Single-
637   Molecule Anisotropy Imaging. *Biophys. J.* **77**, 2864–2870.

638 **Harms, G. S., Cognet, L., Lommerse, P. H. M., Blab, G. A. and Schmidt, T.** (2001). Autofluo-
639   rescent Proteins in Single-Molecule Research: Applications to Live Cell Imaging Mi-
640   croscopy. *Biophys. J.* **80**, 2396–2408.

641 **Hobbs, G. A., Der, C. J. and Rossman, K. L.** (2016). RAS isoforms and mutations in cancer at a
642   glance. *J. Cell Sci.* **129**, 1287–1292.

643 **Jacobson, K., Liu, P. and Lagerholm, B. C.** (2019). The Lateral Organization and Mobility of
644   Plasma Membrane Components. *Cell* **177**, 806–819.

645 **Kaufman, C. K., Mosimann, C., Fan, Z. P., Yang, S., Thomas, A. J., Ablain, J., Tan, J. L.,**
646   **Fogley, R. D., Rooijen, E. van, Hagedorn, E. J., et al.** (2016). A zebrafish melanoma
647   model reveals emergence of neural crest identity during melanoma initiation. *Science*
648   **351**,.

649   **Kawakami, A., Fukazawa, T. and Takeda, H.** (2004). Early fin primordia of zebrafish larvae
650   regenerate by a similar growth control mechanism with adult regeneration. *Dev. Dyn.*
651   **231**, 693–699.

652   **Kusumi, A., Sako, Y. and Yamamoto, M.** (1993). Confined lateral diffusion of membrane re-
653   ceptors as studied by single particle tracking (nanovid microscopy). Effects of cal-
654   cium-induced differentiation in cultured epithelial cells. *Biophys. J.* **65**, 2021–2040.

655   **Kusumi, A., Fujiwara, T. K., Chadda, R., Xie, M., Tsunoyama, T. A., Kalay, Z., Kasai, R. S. and
656   Suzuki, K. G. N.** (2012). Dynamic Organizing Principles of the Plasma Membrane that
657   Regulate Signal Transduction: Commemorating the Fortieth Anniversary of Singer
658   and Nicolson's Fluid-Mosaic Model. *Annu. Rev. Cell Dev. Biol.* **28**, 215–250.

659   **Lieschke, G. J. and Currie, P. D.** (2007). Animal models of human disease: zebrafish swim
660   into view. *Nat. Rev. Genet.* **8**, 353–367.

661   **Lingwood, D. and Simons, K.** (2010). Lipid Rafts As a Membrane-Organizing Principle. *Sci-
662   ence* **327**, 46–50.

663   **Lommerse, P. H. M., Blab, G. A., Cognet, L., Harms, G. S., Snaar-Jagalska, B. E., Spaink, H. P.
664   and Schmidt, T.** (2004). Single-Molecule Imaging of the H-Ras Membrane-Anchor Re-
665   veals Domains in the Cytoplasmic Leaflet of the Cell Membrane. *Biophys. J.* **86**, 609–
666   616.

667   **Lommerse, P. H. M., Snaar-Jagalska, B. E., Spaink, H. P. and Schmidt, T.** (2005). Single-mole-
668   cule diffusion measurements of H-Ras at the plasma membrane of live cells reveal
669   microdomain localization upon activation. *J. Cell Sci.* **118**, 1799–1809.

670   **Lommerse, P. H. M., Vastenhoud, K., Pirinen, N. J., Magee, A. I., Spaink, H. P. and Schmidt,
671   T.** (2006). Single-Molecule Diffusion Reveals Similar Mobility for the Lck, H-Ras, and
672   K-Ras Membrane Anchors. *Biophys. J.* **91**, 1090–1097.

673   **Malumbres, M. and Barbacid, M.** (2003). RAS oncogenes: the first 30 years. *Nat. Rev. Cancer*
674   **3**, 459–465.

675 **Murakoshi, H., Iino, R., Kobayashi, T., Fujiwara, T., Ohshima, C., Yoshimura, A. and Kusumi,**
676   **A.** (2004). Single-molecule imaging analysis of Ras activation in living cells. *Proc. Natl.*
677   *Acad. Sci.* **101**, 7317–7322.

678 **Nickels, J. D., Smith, J. C. and Cheng, X.** (2015). Lateral organization, bilayer asymmetry, and
679   inter-leaflet coupling of biological membranes. *Chem. Phys. Lipids* **192**, 87–99.

680 **Pezzarossa, A., Zosel, F. and Schmidt, T.** (2015). Visualization of HRas Domains in the Plasma
681   Membrane of Fibroblasts. *Biophys. J.* **108**, 1870–1877.

682 **Plowman, S. J., Muncke, C., Parton, R. G. and Hancock, J. F.** (2005). H-ras, K-ras, and inner
683   plasma membrane raft proteins operate in nanoclusters with differential dependence
684   on the actin cytoskeleton. *Proc. Natl. Acad. Sci.* **102**, 15500–15505.

685 **Prior, I. A., Muncke, C., Parton, R. G. and Hancock, J. F.** (2003). Direct visualization of Ras
686   proteins in spatially distinct cell surface microdomains. *J. Cell Biol.* **160**, 165–170.

687 **Reisser, M., Palmer, A., Popp, A. P., Jahn, C., Weidinger, G. and Gebhardt, J. C. M.** (2018).
688   Single-molecule imaging correlates decreasing nuclear volume with increasing TF-
689   chromatin associations during zebrafish development. *Nat. Commun.* **9**, 5218.

690 **Rotblat, B., Prior, I. A., Muncke, C., Parton, R. G., Kloog, Y., Henis, Y. I. and Hancock, J. F.**
691   (2004). Three Separable Domains Regulate GTP-Dependent Association of H-ras with
692   the Plasma Membrane. *Mol. Cell. Biol.* **24**, 6799–6810.

693 **Schaaf, M. J. M., Koopmans, W. J. A., Meckel, T., van Noort, J., Snaar-Jagalska, B. E.,**
694   **Schmidt, T. S. and Spaink, H. P.** (2009). Single-Molecule Microscopy Reveals Mem-
695   brane Microdomain Organization of Cells in a Living Vertebrate. *Biophys. J.* **97**, 1206–
696   1214.

697 **Schütz, G. J., Schindler, H. and Schmidt, T.** (1997). Single-molecule microscopy on model
698   membranes reveals anomalous diffusion. *Biophys. J.* **73**, 1073–1080.

699 **Seefeldt, B., Kasper, R., Seidel, T., Tinnefeld, P., Dietz, K.-J., Heilemann, M. and Sauer, M.**
700   (2008). Fluorescent proteins for single-molecule fluorescence applications. *J. Biopho-*
701   *tonics* **1**, 74–82.

702   **Semrau, S. and Schmidt, T.** (2007). Particle Image Correlation Spectroscopy (PICS): Ret-

703   rieving Nanometer-Scale Correlations from High-Density Single-Molecule Position

704   Data. *Biophys. J.* **92**, 613–621.

705   **Simons, K. and Gerl, M. J.** (2010). Revitalizing membrane rafts: new tools and insights. *Nat.*

706   *Rev. Mol. Cell Biol.* **11**, 688–699.

707   **Singer, S. J. and Nicolson, G. L.** (1972). The Fluid Mosaic Model of the Structure of Cell Mem-

708   branes. *Science* **175**, 720–731.

709   **Willumsen, B. M., Christensen, A., Hubbert, N. L., Papageorge, A. G. and Lowy, D. R.** (1984).

710   The p21 ras C-terminus is required for transformation and membrane association.

711   *Nature* **310**, 583–586.

712

713 **FIGURES**

714

715
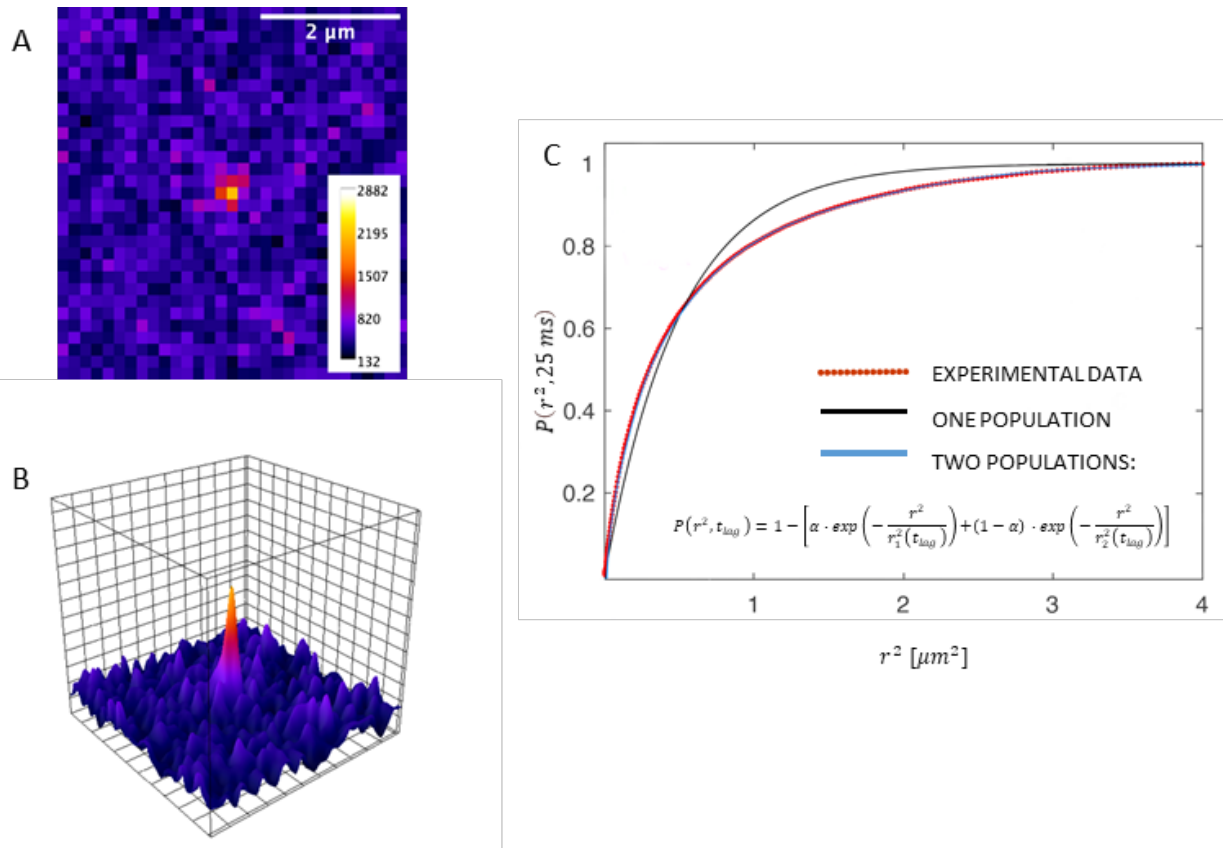
716 *FIGURE 1. Single-Molecule Microscopy (SMM) analysis of protein localization and mobility.* **(A)** *SMM intensity map showing signal of a YFP-C10H-Ras molecule located in the basal membrane of a HEK29T cell.* **(B)** *3D representation of the image shown in (A), depicting fluorescence intensities of each pixel. One visible intensity peak is shown that can be attributed to a single YFP-C10H-Ras molecule. Over these peaks, two-dimensional Gaussian surfaces were fitted.* **(C)** *Representative cumulative distribution plot of squared displacements determined using PICS analysis. Data are shown in red, and plots are best using a two populations biexponential model (in blue, formula shown). Fitting of the data points to the two populations model allows for calculation of a relative size of the subpopulations (α) and their mean squared displacements (r_1^2 and r_2^2). This procedure was repeated for each of the time lags used.*

717
718
719
720
721
722
723
724
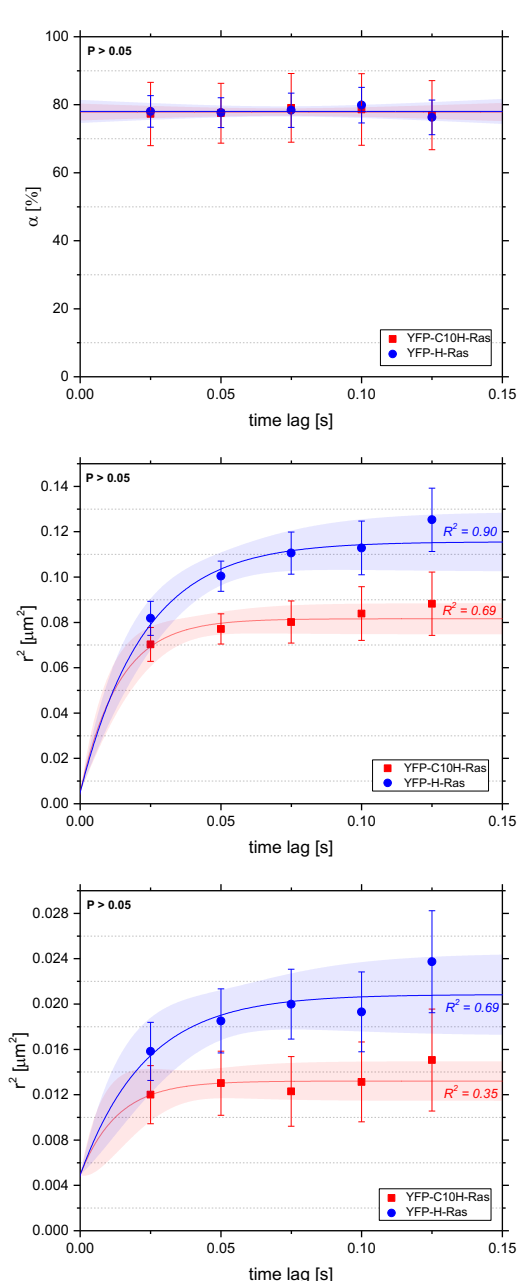
FIGURE 2. Mobility patterns of YFP-C10H-Ras and YFP-H-Ras in HEK293T cells. *(A) Fraction size of the fast-diffusing population, plotted against the time lag. (B) Mean squared displacements plotted against the time lag for the fast-diffusing fraction. (C) Mean squared displacements plotted against the time lag for the slow-diffusing fraction. Results of the fits are summarized in Table 1. Statistical analysis was performed using an unpaired t-test. Pearson correlation coefficients R^2 are presented to show fitness of the data to the model of confined diffusion.*
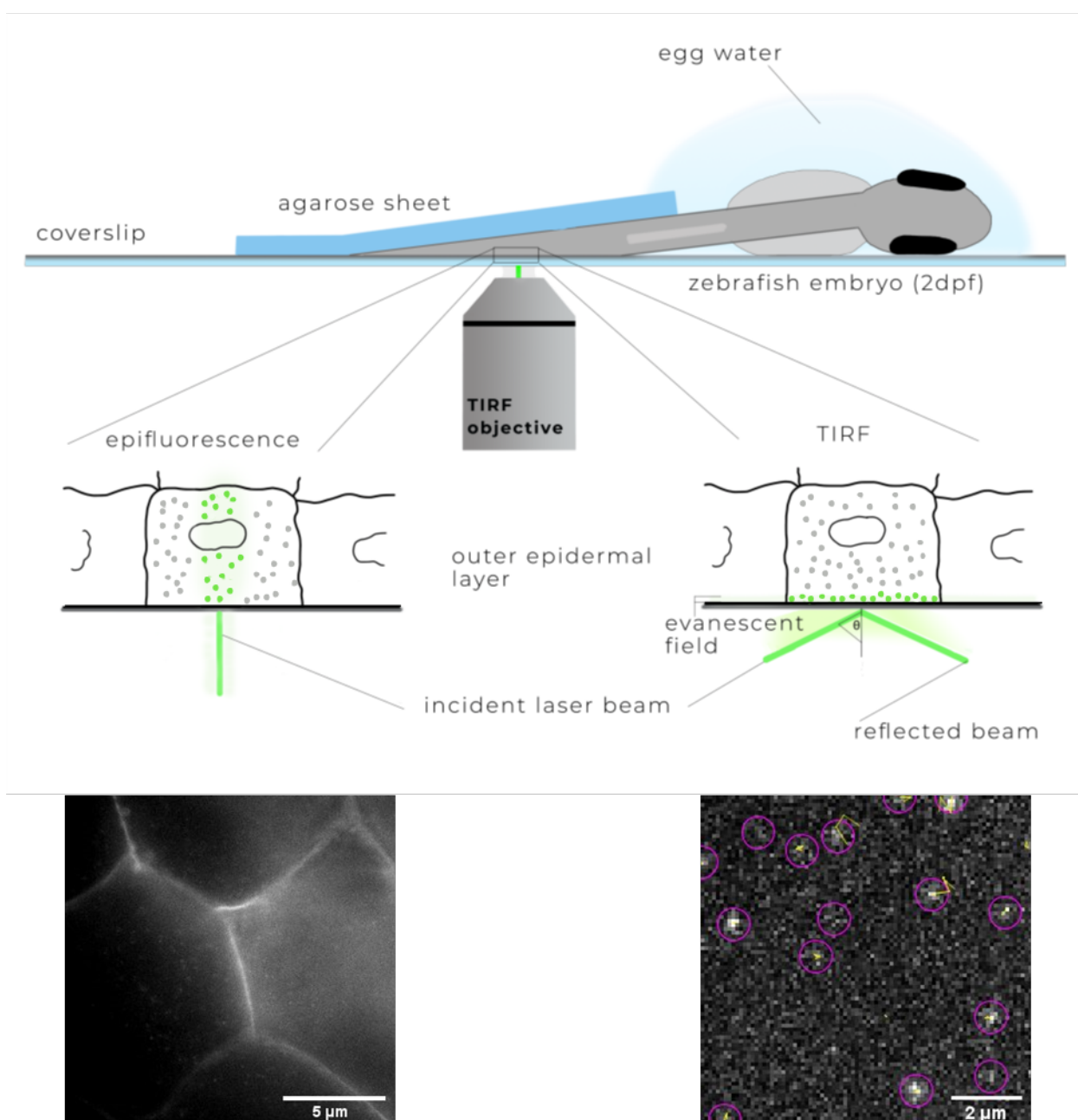
FIGURE 3. Schematic overview of SMM applied to a living zebrafish embryo. *A zebrafish embryo was injected with an expression vector for a YFP fusion protein shortly after fertilization. At 2 dpf, it was placed on a coverslip coated with poly-L-lysine in a drop of egg water. The tail region of the embryo was covered with a 0.75-mm-thick agarose sheet. On the lower left part of the figure, an epifluorescence picture is presented of the outer layer of the epidermis showing the fluorescent signal of YFP-C10-H-Ras in the cell membranes. On the lower right, a TIRFM image from the same FOV is presented, with examples of individual YFP molecules shown in circles and their trajectories in yellow.*
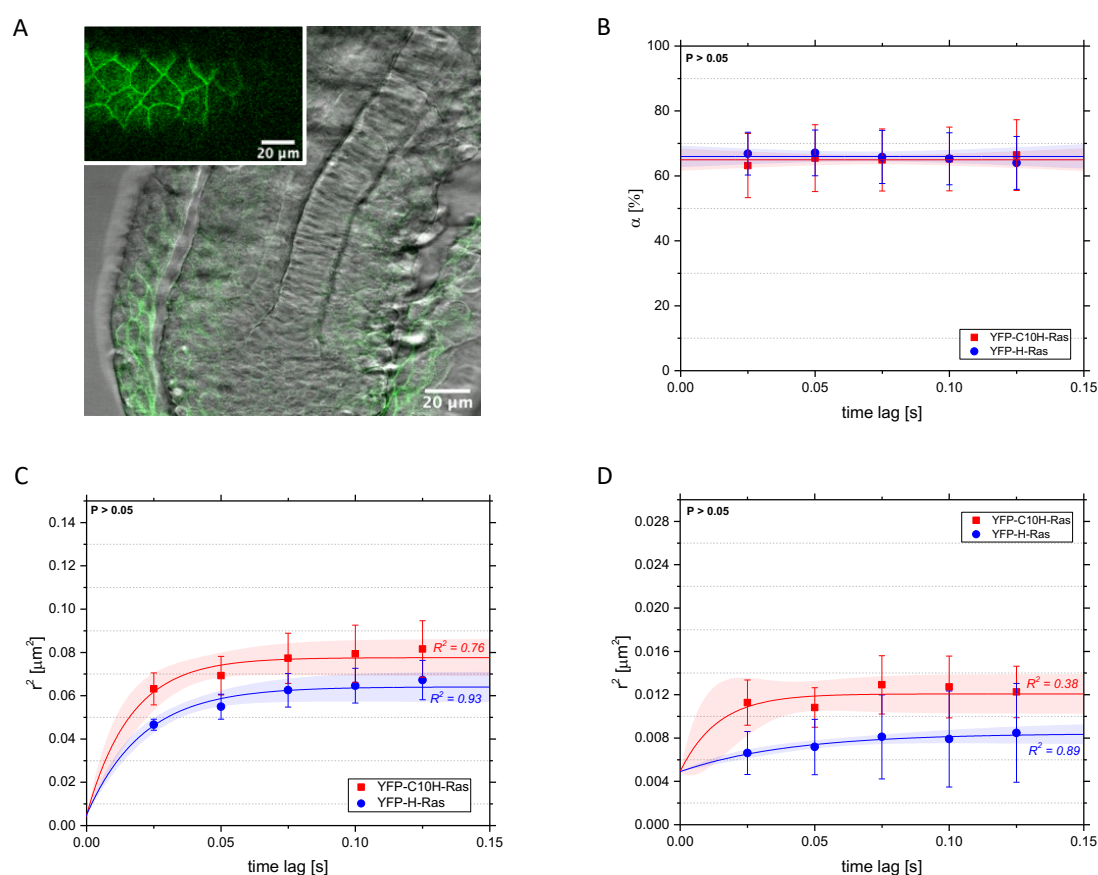
FIGURE 4. **Mobility patterns of YFP-C10H-Ras and YFP-H-Ras in epidermal cells of the zebrafish embryos**. *(A) Overlay of brightfield and fluorescence microscopy image of the zebrafish embryo epidermal cell layer expressing GFP-C10H-Ras at 2 dpf (GFP-C10H-Ras transgenic line). The image shows that the embryonic epidermis consists of a homogenous cell population. Inset shows fluorescence microscopy image depicting a part of the zebrafish tail fin membrane. (B) Fraction size of the fast-diffusing population, plotted against the time lag. (C) Mean squared displacements plotted against the time lag for the fast-diffusing fraction. (D) Mean squared displacements plotted against the time lag for the slow-diffusing fraction. Results of the fits are summarized in Table 1. Statistical analysis was performed using an unpaired t-test. Pearson correlation coefficients R^2 are presented to show fitness of the data to the model of confined diffusion.*
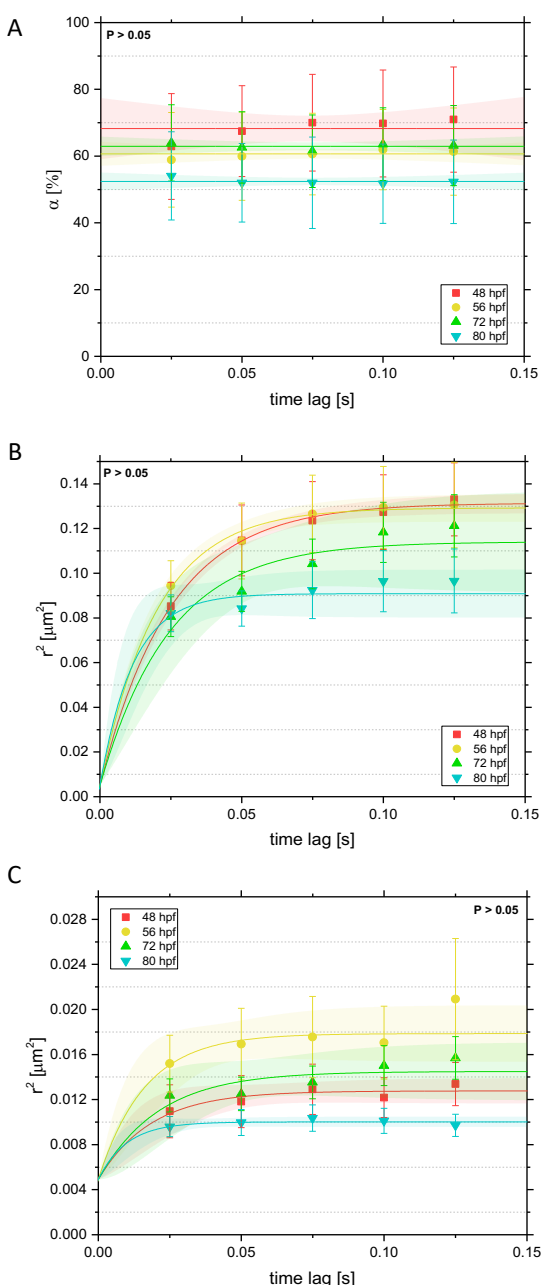
735

736

737

738

739

740

741

742

743

744

745

746
747
748
749

FIGURE 5. Mobility patterns of YFP-C10H-Ras in epidermal cells of the zebrafish embryos at different developmental stages. *(A) Fraction size of the fast-diffusing population, plotted against the time lag. (B) Mean squared displacements plotted against the time lag for the fast-diffusing fraction. (C) Mean squared displacements plotted against the time lag for the slow-diffusing fraction. Results of the fits are summarized in Table 1. Statistical analysis was performed, using a one-way ANOVA.*
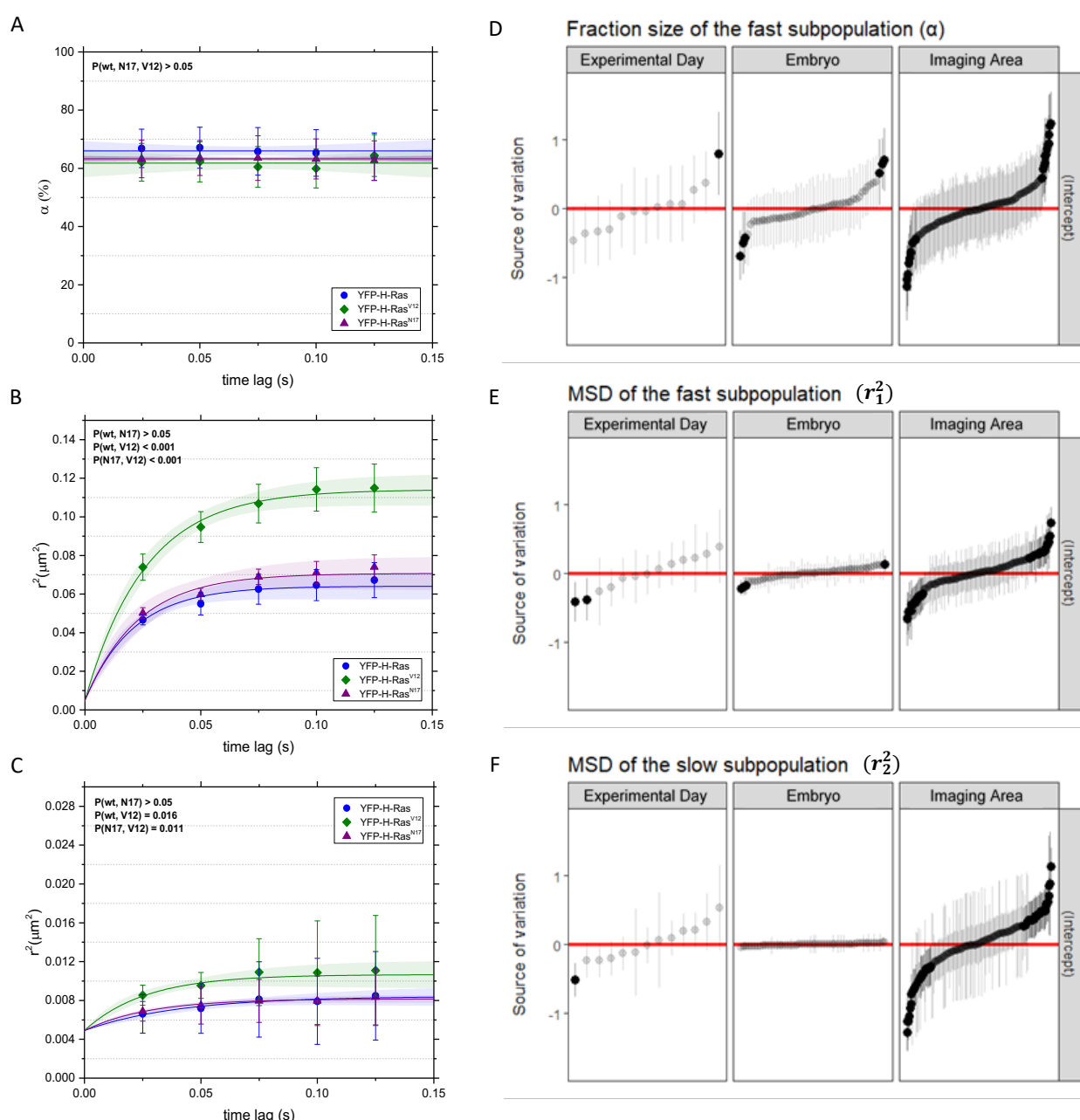
FIGURE 6: Mobility patterns of YFP-H-Ras and its mutants, YFP-H-Ras^{V12} and YFP-H-Ras^{N17}, in epidermal cells of the zebrafish embryos at different developmental stages. *(A) Fraction size of the fast-diffusing population, plotted against the time lag. (B) Mean squared displacements plotted against the time lag for the fast-diffusing fraction. (C) Mean squared displacements plotted against the time lag for the slow-diffusing fraction. Results of the fits are summarized in Table 1.. Statistical analysis was performed, using a one-way ANOVA. (D, E, F) Caterpillar plots presenting the effect range of a different experimental day, different embryos within an experimental day, and different areas within an embryo to an overall variability in the fast-diffusing fraction size (D), mean squared displacement of the fast-diffusing fraction (E), and slow-diffusing fraction (F). Effect ranges represent the relative deviation of group intercepts from the overall mean with 95% confidence intervals. Red lines indicate the overall mean of the data, while black points signify groups that significantly deviate from the overall mean among batches, individual embryos, and areas. The data points are sorted based on their deviation from the total average, with the ones most negatively deviating placed on the left. The values in (D) were logit-transformed and the values in (E) and (F) were logarithm-transformed, to meet the statistical hypotheses of the hierarchical linear model.*